Journal of chemical & engineering data

Article

Cite This: J. Chem. Eng. Data 2019, 64, 5814−5823

pubs.acs.org/jced

# Effects of Activation Temperature and Densification on Adsorption Performance of MOF MIL-100(Cr)

Jiangfeng Yang,[†,‡] Honghao Bai,[†] Feifei Zhang,[†] Jiaqi Liu,[†] Joseph Winarta,[§] Yong Wang,[‡] and Bin Mu*[,§]

[†]Research Institute of Special Chemicals, College of Chemistry and Chemical Engineering and [‡]Shanxi Key Laboratory of Gas Energy Efficient and Clean Utilization, Taiyuan University of Technology, Taiyuan 030024, Shanxi, P. R. China

[§]Chemical Engineering, School for Engineering of Matter, Transport, and Energy, Arizona State University, 501 East Tyler Mall, Tempe, Arizona 85287, United States

*Supporting Information*

**ABSTRACT:** Metal−organic frameworks (MOFs) with open metal sites have attracted lots of attention because of their high binding energy for adsorbates. MIL-100(Cr) is one of the potential MOFs for challenging separations. Multicomponent breakthrough studies on MOF pellets are critically needed because only pelletized adsorbents can be used in pressure or temperature swing adsorption processes. Thus, in this study, we compared the adsorption equilibrium of MIL-100(Cr) powder and pellets and carried out a breakthrough study of multicomponent gas mixtures on pelletized MIL-100(Cr), which revealed interesting effects of activation conditions on its performance. The experimental results show that the $CO_2$ adsorption capacity of MIL-100(Cr) powder activated at 523 K and high vacuum ($10^{-10}$ bar) was about 2.5 times higher than that of MIL-100(Cr) treated under mild activation conditions (423 K). The highest 5.8 mol/g $CO_2$ capacity at 298 K and 1 bar is consistent with the high $CO_2$−$Cr^{3+}$ binding energy of 63 kJ/mol, determined using density functional theory calculations. However, the number drops to 4.05 mol/g for pelletized samples. The negative impact of densification on the adsorption capacity follows the order of $CO_2 > N_2 > CH_4$ for MIL-100(Cr)250 and $CH_4 > N_2 > CO_2$ for MIL-100(Cr)150, which also suggests that the effects of open Cr sites on the adsorption capacity follows the order of $CO_2 > N_2 > CH_4$ on MIL-100(Cr). The selectivity of MIL-100(Cr) pellets based on breakthrough measurements for $CO_2/N_2$ (20/80) and $CO_2/CH_4$ (40/60) mixtures was 4.3 and 10.7, respectively.

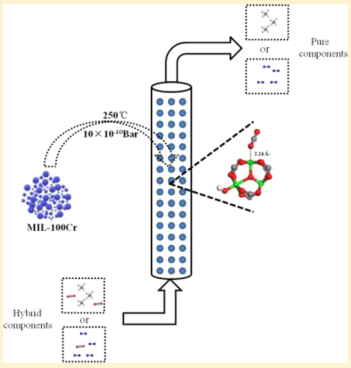


## 1. INTRODUCTION

Among different $CO_2$ emission sources, flue gas with a $CO_2$ concentration less than 20% is the largest single-source contributor, and thus selective capture of $CO_2$ is essential to reduce $CO_2$ emission.[1−5] In addition, removing $CO_2$ from $CH_4$ is important to upgrade the quality of biogas and natural gas and to reduce pipeline corrosion issues.[6−10] At present, most industrial processes are still using chemical absorption with amine solutions for $CO_2$ capture, which shows high efficiency but suffers from high energy regeneration costs and issues with severe corrosion of equipment and pipelines.[11−15] Among different $CO_2$ capture technologies, physical adsorption using porous materials is a promising, cost-efficient method, particularly for low to medium-volume capture by using a pressure swing adsorption process.[6,10] Zeolites,[16−18] porous carbon,[19−22] and nanotubes[23,24] have been screened and examined for their selective adsorption behavior,[25−27] regeneration issues,[28] and kinetics for $CO_2$ separation performance.[29−35] Metal−organic frameworks (MOFs) have also attracted much attention for $CO_2$ capture.[36−39] The $CO_2$ uptake capacities of many MOFs are much higher than those of traditional porous materials due to their high surface area and versatile chemical properties.[40−42] Abundant adsorption sites on the surface can significantly enhance the overall performance;[43−46] therefore, functionalized MOFs with many stronger adsorption sites have been demonstrated by, for instance, grafting amine groups onto MOFs to improve their affinity to $CO_2$ molecules.[47−51] However, due to the gradual loss of the external amine groups during multiple adsorption−desorption cycles, the cycling performance of these modified materials is generally poor.

MOFs with unsaturated metal sites (open metal sites) have received much more attention than other MOFs due to their intrinsic binding sites.[43−45,52−54] These specific MOFs include MIL-101/100,[55] HKUST-1,[56] and MOF-74 (CPO-27),[43] and so on. Murray et al. synthesized Cr-BTC with the same structure of HKUST-1 (Cu-BTC), having an oxygen capacity of up to 11 wt % (3.4 mol/g). The extremely high $O_2$ adsorption on Cr-BTC was attributed to the redox activity of the open Cr sites.[45] Bloch et al. found that Fe-MOF-74 has a high $O_2/N_2$ selectivity due to the electron transfer interactions. Similar to Cr-BTC, the unsaturated $Fe^{2+}$ metal center provides strong binding sites for adsorption and separation.[43,57,58]

**Received:** August 7, 2019
**Accepted:** October 9, 2019
**Published:** October 22, 2019







DOI: 10.1021/acs.jced.9b00770
J. Chem. Eng. Data 2019, 64, 5814−5823

MIL-100/101 have a higher water stability than HKUST-1 and MOF-74 and therefore hold a high potential for practical applications. However, our understanding of the effects of open $Cr^{3+}$ sites on adsorption is still very limited. A recent study reveals that the activation of MIL-100(Cr) at 523 K and a high vacuum (less than $10^{-5}$ torr) can expose the $Cr^{3+}$ sites to achieve high $N_2/CH_4$ selectivity.[59] Our own study also reveals that MIL-100(Cr) activated at similar conditions has an incremental adsorption of $N_2$ and $N_2O$ because the $Cr^{3+}$ sites are exposed after removing the coordinated water molecules, in which the binding energy of $N_2O$ on the open $Cr^{3+}$ sites of MIL-100(Cr) was up to 72.5 kJ/mol, and the $N_2O$ adsorption capacity is similar to that of $CO_2$.[60] These preliminary studies have demonstrated very intriguing properties of open $Cr^{3+}$ sites in MIL-100(Cr).

In addition, the densification of adsorbent materials by forming pellets, extrudates, or beads is essential to improve the mechanical and thermal properties of adsorbent materials and lower the bed pressure drop for industrial pressure or temperature swing adsorption processes.[61,62] However, most of the previous studies of MIL-100(Cr) are based on the fine powder form, and several publications reported MIL-100(Cr) monoliths for hydrogen storage and water adsorption.[63−66] Therefore, in this work, we studied the effects of activation temperature on the adsorption behavior of MIL-100(Cr) pellets, in which multicomponent $CO_2/CH_4$ and $CO_2/N_2$ kinetic separation performance was investigated in detail.

## 2. EXPERIMENTAL SECTION

**2.1. Synthesis of MIL-100(Cr) Crystals.** MIL-100(Cr) was synthesized in our laboratory according to the reported procedure:[67,68] A mixture of powdered Cr (0.104 g), $H_3BTC$ (0.3 g), HF (40%, 0.2 mL), and $H_2O$ (9.6 mL) was added into a Teflon-lined autoclave and heated from room temperature to 493 K in 12 h and kept at 493 K for 4 days. The synthesis is presented in Table 1. After cooling to the ambient temperature naturally, the green powder was collected by repeated centrifugation and thorough washing by distilled water.

**Table 1. Synthesis Condition of MIL-100(Cr)**

| reactants | name | chemical formula | amount (mmol) |
|---|---|---|---|
| | elementary chromium | Cr | 2 |
| | trimesic acid ($H_3BTC$) | $C_9H_6O_6$ | 1.5 |
| | hydrofluoric acid | HF | 4.5 |
| | deionized water | $H_2O$ | 533 |
| reaction temperature | 493 K | | |
| reaction time | 4 days | | |

**2.2. Preparation of MIL-100(Cr) Pellets.** The synthesized MIL-100(Cr) was sufficiently ground in a mortar to obtain a fine powder, and then the powder was added into a tableting machine and extruded into a sheet under a pressure of 4 MPa. It should be noted that the MOF powder added to the tableting machine should not be excessive as it may cause the strength of the pressed MOF sheet to decrease and lead to serious particle pulverization in the later stage. The pressed MOF sheet was suitably pulverized and then passed through a 40−60 mesh steel wire screen to obtain MOF particles having a diameter of about 1 mm. Scheme 1 demonstrates the preparation process of MOF pellets, while Figure 1 shows the final MIL-100(Cr) pellets.

**2.3. Sample Activation.** The MIL-100(Cr) samples including powder and pellet forms were activated under a high vacuum ($10^{-10}$ bar) at different temperatures (373, 423, 473, 523, and 573 K) for 12 h on the degasser unit of ASAP 2460 and named MIL-100(Cr)100/150/200/250/300, respectively.

**2.4. Adsorption Isotherms.** All adsorption isotherms of single-component gas ($CO_2$, $CH_4$, $N_2$) were obtained using a Micromeritics ASAP 2460 instrument; the instrument's uncertainty is ±0.05%. The samples were outgassed at high temperatures (from 373 to 573 K) and high vacuum ($10^{-10}$ bar) for 12 h. The isotherms were collected at 298 K and up to 1 bar.

**2.5. Calculation of Binding Energy.** Cluster models for MIL-100(Cr) were prepared from the diffraction experiments and used as the initial models. The dangling bonds on these fragmented clusters were terminated by methyl ($CH_3$) groups to maintain the correct hybridization.[69] We calculated the binding energy of $CO_2$ with Cr-MOF using density functional theory (DFT) in Dmol3.[70] The gradient corrected approximation treated using the Perdew−Burke−Ernzerhof exchange−correlation potential with long-range dispersion correction via Grimme's scheme was used in all our calculations.[71,72] A real-space orbital global cut off of 3.7 Å was applied and the convergence threshold parameters for the optimization were $10^{-5}$ (energy), $2 \times 10^{-3}$ (gradient), and $5 \times 10^{-3}$ (displacement).[73] Double numeric polarization was used as the basis set. The DFT semicore pseudopots,[74] which were developed specifically for DMol3 calculations, were used to set the type of core treatment. The self-consistent field (SCF) procedure was used with a convergence threshold of $10^{-6}$ au on the energy and electron density. The direct inversion of the iterative subspace technique developed by Pulay was used with a subspace size 6 to speed up the SCF convergence in these systems.[75]

**2.6. Breakthrough Experiment of Mixed Gases.** The mixed-gas breakthrough experiments were carried out in a fixed-bed separation device developed by our research group.[76] The device was composed of displacement gas (He, 99.999%), mixed gas at different volume ratios ($CO_2/N_2$ 20/80% and

**Scheme 1. Preparation of MOF Pellets Including Tableting, Extruding, Crushing, and Sieving Steps**

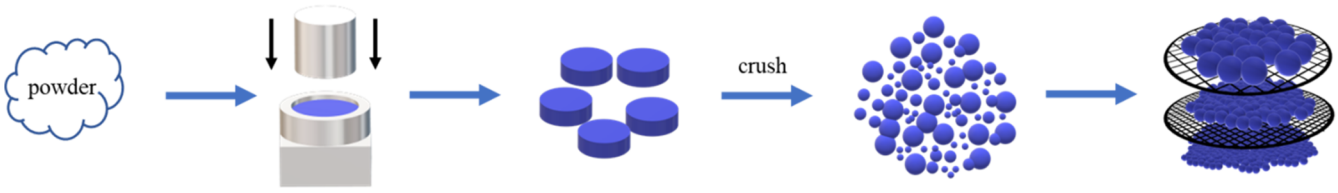




DOI: 10.1021/acs.jced.9b00770
J. Chem. Eng. Data 2019, 64, 5814−5823

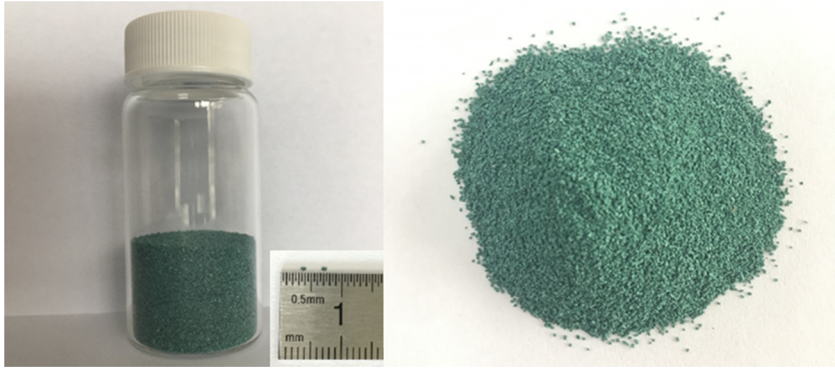


**Figure 1.** MIL-100(Cr) particles through a 40−60 mesh sieve present an average diameter of about 1 mm. These pellets were used for the adsorption isotherm and breakthrough measurements.

$CO_2/CH_4$ 40/60%), mass flow meter (5 mL/min), adsorption column (inner diameter × length: 9 mm × 150 mm), pressure change valve, pressure gauge, and gas chromatograph. The adsorption column filled with MIL-100(Cr) pellets was loaded into the testing device. High-purity helium gas was then used to purge the adsorption column until no other gases were detected at the end of the adsorption column and the purification step was complete. Then the carrier gas was stopped, and the testing gas valve was opened. The conditions were controlled at normal pressure and the gas flow rate was set at 5 mL/min for 5−10 min. After the flow rate was stabilized, the gas was introduced into the adsorption column and the outlet gas was collected and analyzed using gas chromatography (Shimadzu UG2014C). From the analysis of the content of the gas components obtained with time, the gas permeation curve was obtained.

The gas uptake by the adsorbents, represented as $Q_t$ (mmol/g), is determined by the following equation

$$Q_t = \frac{v\int_0^{\infty}[c_{i,0} - c_i(t)]\mathrm{d}t}{m}$$

The selectivity $S$ is estimated by the following equation

$$S_{i/j} = \frac{Q_i/x_i}{Q_j/x_j}$$

where $v$ is the flow rate of pure gas in mL/min, $m$ is the mass of the adsorbent sample in g, $t$ is time taken for adsorption in minutes, $C_0$ and $C$ are concentrations of gas at inlet and outlet, respectively, in mmol/mL, and $x$ is the gas volume fraction.

## 3. RESULTS AND DISCUSSION

**3.1. Effects of Activation Temperature on $CO_2$ Uptake of MIL-100(Cr).** The adsorption isotherms of $CO_2$ at 298 K and 1 bar on MIL-100(Cr) powder samples activated at different temperatures are shown in Figure 2, and the data are listed in Table 2, in which the adsorption capacity of $CO_2$ significantly increases with the activation temperature from MIL-100(Cr)100 to MIL-100(Cr)300, up to 6.09 mmol/g, showing a 250% increase. The powder X-ray diffraction (XRD) patterns of MIL-100(Cr) samples are provided in Figure S1, in which all activated samples show the sample peak positions. However, the peak height of MIL-100(Cr)300 samples is a little lower than that of other samples, indicating that 575 K for 12 h may damage the MOF crystallinity a little. The $N_2$ isotherms at 77 K (Figure S2) also clearly show that samples activated at a higher temperature have a higher surface area than those activated at a lower temperature. Interestingly, the enhancement of the adsorption capacity with increased activation temperature was not even. As shown in Figure 2, the increase from 373 K (MIL-100(Cr)100) to 432 K (MIL-100(Cr)150) or from 523 K (MIL-100(Cr)250) to 575 K (MIL-100(Cr)300) only enhances the update a little, while the biggest improvement is between MIL-100(Cr)200 and MIL-

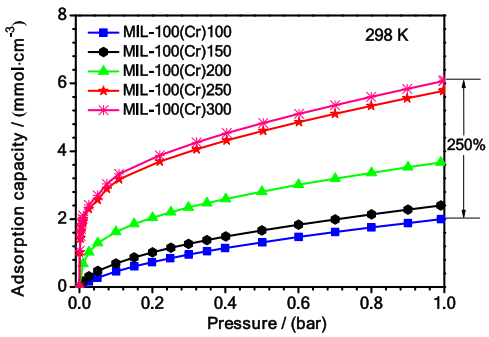


**Figure 2.** Adsorption isotherms of $CO_2$ at 298 K on MIL-100(Cr) activated at 373−573 K.

**Table 2. Adsorption Data of $CO_2$ at 298 K on MIL-100(Cr) Powder Sample Activated at 373−573 K**

| | capacity (mmol/g) | | | | |
|---|---|---|---|---|---|
| pressure (bar) | MIL-100(Cr) 100 | MIL-100(Cr) 150 | MIL-100(Cr) 200 | MIL-100(Cr) 250 | MIL-100(Cr) 300 |
| 0.01009 | 0.07179 | 0.16577 | 0.68127 | 2.00167 | 2.10175 |
| 0.02626 | 0.16600 | 0.31549 | 1.02605 | 2.30302 | 2.41817 |
| 0.04954 | 0.27303 | 0.47261 | 1.29516 | 2.57200 | 2.70060 |
| 0.10082 | 0.45917 | 0.69511 | 1.62427 | 2.89463 | 3.03937 |
| 0.15063 | 0.60755 | 0.87177 | 1.85658 | 3.17289 | 3.33153 |
| 0.19904 | 0.73126 | 1.02150 | 2.04258 | 3.69678 | 3.88162 |
| 0.24916 | 0.84691 | 1.15644 | 2.20600 | 3.80105 | 4.00468 |
| 0.29938 | 0.95382 | 1.26952 | 2.34386 | 3.98829 | 4.17554 |
| 0.34998 | 1.05354 | 1.37891 | 2.47255 | 4.14511 | 4.34874 |
| 0.39958 | 1.14635 | 1.48789 | 2.59288 | 4.31974 | 4.53572 |
| 0.50136 | 1.31705 | 1.66850 | 2.80879 | 4.60231 | 4.83242 |
| 0.60069 | 1.47232 | 1.83570 | 3.01272 | 4.85786 | 5.10075 |
| 0.70106 | 1.61760 | 1.99138 | 3.19068 | 5.10083 | 5.35587 |
| 0.80041 | 1.75418 | 2.13854 | 3.36100 | 5.33439 | 5.60111 |
| 0.90041 | 1.88406 | 2.27981 | 3.52908 | 5.55902 | 5.83697 |
| 0.99075 | 1.99898 | 2.40174 | 3.67189 | 5.80235 | 6.09247 |


DOI: 10.1021/acs.jced.9b00770
J. Chem. Eng. Data 2019, 64, 5814−5823

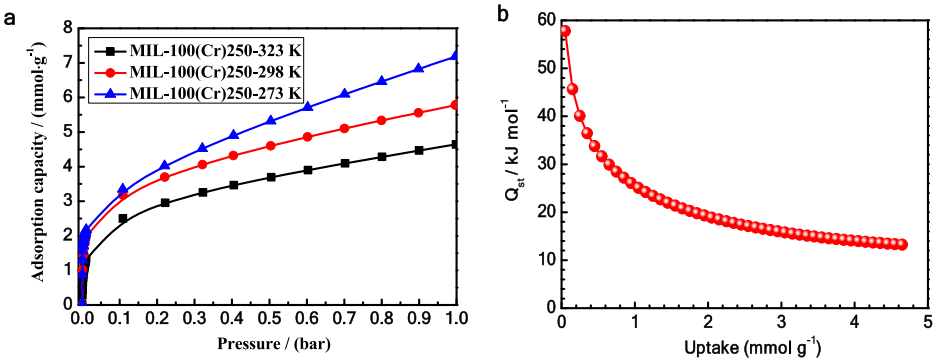


**Figure 3.** (a) Adsorption isotherms of $CO_2$ on MIL-100(Cr)250 at 273, 298, and 323 K and (b) the adsorption heat of $CO_2$.

**Table 3. Adsorption Update of $CO_2$ on MIL-100(Cr)250 Powder Sample at 273, 298, and 323 K, Respectively**

| | capacity (mmol/g) | | |
|---|---|---|---|
| pressure (bar) | 323 K | 298 K | 273 K |
| 0.01038 | 1.32824 | 2.00158 | 2.17682 |
| 0.10878 | 2.49797 | 3.17275 | 3.34766 |
| 0.22165 | 2.95530 | 3.69662 | 4.02190 |
| 0.32266 | 3.25259 | 4.05805 | 4.52142 |
| 0.40483 | 3.46443 | 4.31955 | 4.89915 |
| 0.50480 | 3.69255 | 4.60211 | 5.31779 |
| 0.60325 | 3.90027 | 4.85765 | 5.71096 |
| 0.70244 | 4.09536 | 5.10061 | 6.09361 |
| 0.80111 | 4.28278 | 5.33416 | 6.46177 |
| 0.89993 | 4.46497 | 5.55878 | 6.82401 |
| 0.99886 | 4.63900 | 5.80210 | 7.18040 |

**Table 4. Adsorption Heat of $CO_2$ on MIL-100(Cr)250 Powder Sample**

| uptake (mmol/g) | adsorption heat (kJ/mol) | uptake (mmol/g) | adsorption heat (kJ/mol) |
|---|---|---|---|
| 0.05 | 57.78685 | 2.05 | 18.89002 |
| 0.15 | 45.66196 | 2.15 | 18.48793 |
| 0.25 | 40.08960 | 2.25 | 18.11037 |
| 0.35 | 36.46114 | 2.35 | 17.75524 |
| 0.45 | 33.78230 | 2.45 | 17.42070 |
| 0.55 | 31.66835 | 2.55 | 17.10514 |
| 0.65 | 29.92948 | 2.65 | 16.80713 |
| 0.75 | 28.45798 | 2.75 | 16.52540 |
| 0.85 | 27.18678 | 2.85 | 16.25882 |
| 0.95 | 26.07131 | 2.95 | 16.00638 |
| 1.05 | 25.08040 | 3.05 | 15.76715 |
| 1.15 | 24.19142 | 3.15 | 15.54032 |
| 1.25 | 23.38742 | 3.25 | 15.32513 |
| 1.35 | 22.65535 | 3.35 | 15.12092 |
| 1.45 | 21.98499 | 3.45 | 14.92706 |
| 1.55 | 21.36813 | 3.55 | 14.74298 |
| 1.65 | 20.79815 | 3.65 | 14.56817 |
| 1.75 | 20.26956 | 3.75 | 14.40215 |
| 1.85 | 19.77780 | 3.85 | 14.24448 |
| 1.95 | 19.31904 | 3.95 | 14.09476 |

100(Cr)250, indicating that the unsaturated Cr centers will not be fully exposed until the activation temperature reaches above 523 K.[63] Thus, in the following experiments, the sample activated at 523 K (MIL-100(Cr)250) is used for most studies.

Two more isotherms were collected on MIL-100(Cr)250 samples for $CO_2$ adsorption at 273 and 323 K, and a comparison is provided in Figure 3a. As shown in the figure, the adsorption quickly occurred at a very low-pressure range (0.01 bar) within the examined temperature range, indicating that the exposed $Cr^+$ is very active towards $CO_2$. With the pressure increase, the effects of adsorption temperature on the uptake started to dominate the isotherm shape and capacity, in

**Table 5. Summary of $CO_2$ Capacity on MIL-100(Cr) at 1 bar**

| | | | activation condition | | | |
|---|---|---|---|---|---|---|
| sorbent | $CO_2$ capacity (mmol/g) | $T$ (K) | $T$ (K) | vacuum (bar) | time (h) | refs |
| MIL-100(Cr) | <1.00 | 298 | 493 | | 1.5 | 52 |
| MIL-100(Cr) | 1.60 | 308 | 373 | 1 | 1.5 | 54 |
| MIL-100(Cr) | 2.11 | 303 | 423 | | | 77 |
| MIL-100(Cr) | 2.60 | 298 | 423 | | 12 | 78 |
| MIL-100(Cr) | 2.67 | 298 | 423 | $1 \times 10^{-10}$ | 12 | 79 |
| MIL-100(Cr) | 3.52 | 303 | 523 | $1 \times 10^{-8}$ | 16 | 80 |
| MIL-100(Cr)/PPD[a] | 1.30 | 298 | 493 | | 1.5 | 52 |
| EN- MIL-100(Cr)[a] | 2.40 | 308 | 373 | 1 | 1.5 | 54 |
| MIL-100(Cr) 150 | 2.06 | 298 | 423 | $1 \times 10^{-10}$ | 12 | |
| MIL-100(Cr) 250 | 4.70 | 323 | 523 | $1 \times 10^{-10}$ | 12 | |
| MIL-100(Cr) 250 | 5.80 | 298 | 523 | $1 \times 10^{-10}$ | 12 | |
| MIL-100(Cr) 250 | 7.18 | 273 | 523 | $1 \times 10^{-10}$ | 12 | |
| MIL-100(Cr) 300 | 6.09 | 298 | 573 | $1 \times 10^{-10}$ | 12 | |

[a]Amine functionalization of MIL-100(Cr).

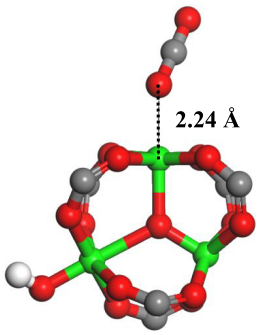


**Figure 4.** DFT calculations for an adsorbed $CO_2$ molecule around the Cr atom in a MIL-100 cluster; $CO_2$−Cr distance is 2.243 Å (chromium, oxygen, carbon, and hydrogen atoms are in green, red, gray, and white, respectively).



DOI: 10.1021/acs.jced.9b00770
J. Chem. Eng. Data 2019, 64, 5814−5823

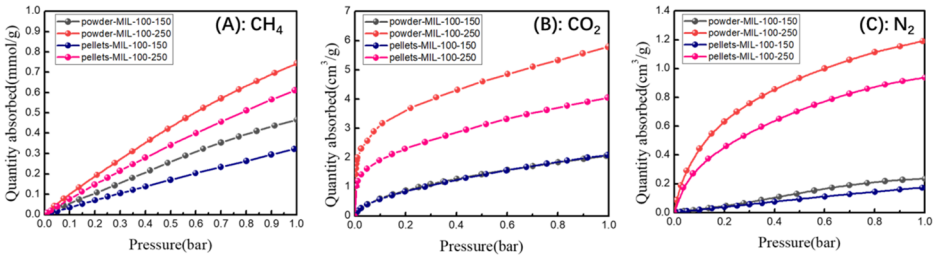


**Figure 5.** Adsorption isotherms of $CH_4$ (A), $CO_2$ (B), and $N_2$ (C) on MIL-100(Cr) samples, including powder and pellets activated at 423 and 523 K, respectively.

**Table 6. Adsorption Data of $CH_4$, $CO_2$, and $N_2$ at 298 K on MIL-100(Cr) Powder Sample Activated at 423 and 523 K, Respectively**

| | capacity (mmol/g) | | | | | |
|---|---|---|---|---|---|---|
| | MIL-100(Cr)150 | | | MIL-100(Cr)250 | | |
| pressure (bar) | $CH_4$ | $CO_2$ | $N_2$ | $CH_4$ | $CO_2$ | $N_2$ |
| 0.01012 | 0.00600 | 0.16325 | 0.00241 | 0.01078 | 1.99590 | 0.08723 |
| 0.02512 | 0.01517 | 0.30836 | 0.00600 | 0.02674 | 2.30017 | 0.18908 |
| 0.05055 | 0.02954 | 0.47308 | 0.01236 | 0.05270 | 2.58469 | 0.29153 |
| 0.10027 | 0.07425 | 0.73581 | 0.03218 | 0.13400 | 3.04549 | 0.44626 |
| 0.15031 | 0.10872 | 0.87156 | 0.04801 | 0.19497 | 3.36878 | 0.54871 |
| 0.20032 | 0.14399 | 1.01901 | 0.06592 | 0.25353 | 3.60430 | 0.63227 |
| 0.25035 | 0.18041 | 1.16032 | 0.08676 | 0.31106 | 3.81421 | 0.70132 |
| 0.30033 | 0.21705 | 1.27794 | 0.11017 | 0.36790 | 3.97908 | 0.75846 |
| 0.35046 | 0.25404 | 1.38414 | 0.13182 | 0.42241 | 4.15827 | 0.80956 |
| 0.40042 | 0.28955 | 1.48946 | 0.15367 | 0.47480 | 4.31597 | 0.85635 |
| 0.49947 | 0.32324 | 1.63077 | 0.17377 | 0.52463 | 4.46650 | 0.93417 |
| 0.59937 | 0.35394 | 1.83089 | 0.19018 | 0.57146 | 4.85152 | 1.00008 |
| 0.69959 | 0.38366 | 1.98976 | 0.20493 | 0.61537 | 5.09830 | 1.05989 |
| 0.80053 | 0.41090 | 2.14248 | 0.21760 | 0.65666 | 5.33762 | 1.11375 |
| 0.89976 | 0.43679 | 2.27238 | 0.22851 | 0.69603 | 5.55939 | 1.15444 |
| 0.98970 | 0.46607 | 2.40140 | 0.23503 | 0.74331 | 5.76536 | 1.19058 |

**Table 7. Adsorption Data of $CH_4$, $CO_2$, and $N_2$ at 298 K on MIL-100(Cr) Pellets Activated at 423 and 523 K, Respectively**

| | capacity (mmol/g) | | | | | |
|---|---|---|---|---|---|---|
| | MIL-100(Cr)150 | | | MIL-100(Cr)250 | | |
| pressure (bar) | $CH_4$ | $CO_2$ | $N_2$ | $CH_4$ | $CO_2$ | $N_2$ |
| 0.01009 | 0.00253 | 0.19047 | 0.00146 | 0.00852 | 1.19874 | 0.04797 |
| 0.02626 | 0.00781 | 0.26646 | 0.00476 | 0.02039 | 1.41664 | 0.17535 |
| 0.04954 | 0.01696 | 0.39725 | 0.01000 | 0.03968 | 1.61924 | 0.27295 |
| 0.10082 | 0.03471 | 0.57207 | 0.01977 | 0.07603 | 1.90436 | 0.37471 |
| 0.15063 | 0.05263 | 0.70774 | 0.02950 | 0.11242 | 2.11360 | 0.46247 |
| 0.19904 | 0.07056 | 0.83501 | 0.03900 | 0.14733 | 2.29649 | 0.53331 |
| 0.24916 | 0.08791 | 1.00200 | 0.04843 | 0.18158 | 2.53239 | 0.59552 |
| 0.29938 | 0.1053 | 1.15838 | 0.05794 | 0.21494 | 2.75095 | 0.65108 |
| 0.34998 | 0.12126 | 1.30094 | 0.06690 | 0.24796 | 2.95100 | 0.70219 |
| 0.39958 | 0.13825 | 1.43735 | 0.07583 | 0.28017 | 3.14029 | 0.74769 |
| 0.50136 | 0.17014 | 1.56611 | 0.09398 | 0.34194 | 3.31490 | 0.78891 |
| 0.60069 | 0.20379 | 1.68122 | 0.11166 | 0.40053 | 3.47706 | 0.82606 |
| 0.70106 | 0.23362 | 1.79208 | 0.12807 | 0.45659 | 3.62751 | 0.85939 |
| 0.80041 | 0.26438 | 1.89651 | 0.14418 | 0.51149 | 3.77465 | 0.88904 |
| 0.90041 | 0.29526 | 1.99604 | 0.15967 | 0.56581 | 3.91123 | 0.9126 |
| 0.99075 | 0.32251 | 2.08968 | 0.17343 | 0.61148 | 4.04699 | 0.93757 |

which three different curves can be distinguished from each other. As expected, the lower adsorption temperature produces a higher uptake curve and the data are provided in Table 3. In addition, we calculated the isosteric heat of adsorption ($Q_{st}$) of $CO_2$ on MIL-100(Cr)250. As shown in Figure 3b and Table 4, the $Q_{st}$ of $CO_2$ at low coverage is up to 58 kJ/mol, which then slowly drops with the uptake, indicating that most active sites have been occupied with the adsorption process.

Here, we summarize the reported $CO_2$ adsorption capacities on MIL-100(Cr) (<4 mmol/g) in Table 5, and the results



DOI: 10.1021/acs.jced.9b00770
J. Chem. Eng. Data 2019, 64, 5814−5823

**Table 8. Summary of Adsorption Capacity of $CH_4$, $CO_2$, and $N_2$ on MIL-100(Cr) Samples**

| samples | $CH_4$ capacity (mmol/g) | $CO_2$ capacity (mmol/g) | $N_2$ capacity (mmol/g) |
|---|---|---|---|
| powder MIL-100(Cr)150 | 0.47 | 2.40 | 0.23 |
| powder MIL-100(Cr)250 | 0.74 | 5.80 | 1.19 |
| pellets MIL-100(Cr)150 | 0.32 | 2.09 | 0.17 |
| pellets MIL-100(Cr)250 | 0.61 | 4.05 | 0.94 |

from this study are among the highest.[77−80] From the above analysis, it seems that three factors are important for the successful activation of MIL-100(Cr): proper temperature (573 K > $T$ > 523 K), high vacuum (<$10^{-10}$ bar), and sufficient activation time (>12 h). Although Hamon et al. found that the $CO_2$ capacity will reach up to 2 mmol/g at low pressure after high-temperature activation, they did not obtain the optimum data due to the lack of high vacuum ($10^{-8}$ bar).[80] Therefore, even functionalized MIL-100(Cr) (MIL-100(Cr)/PPD and EN-MIL-100(Cr)) showed a lower $CO_2$ capacity than MIL-100(Cr)250.[52,54]

In the previous studies, the $CO_2$ adsorption enthalpy on MIL-100(Cr) was determined to be up to 63 kJ/mol.[77] However, most related research reported that MIL-100(Cr) was not a good $CO_2$ removal sorbent candidate due to its low adsorption capacity (<4.0 mmol/g),[52,54,79] which is contradictory to its high adsorption enthalpy. In this work, density functional theory (DFT) calculations estimate that the $CO_2$−Cr distance is 2.243 Å (Figure 4), and the binding energy of $CO_2$ molecules on the open Cr sites on MIL-100(Cr) is about 63 kJ/mol, which is consistent with the previously reported value.[77] In this work, as shown in Figure 3b, the $Q_{st}$ of $CO_2$ at low coverage is up to 58 kJ/mol, close to the calculated binding energy and enthalpy change. Therefore, we believe that the maximum $CO_2$ capacity of MIL-100(Cr) is at least 6.09 mmol/g at 298 K and 1 bar, if the open Cr sites are fully exposed. By comparison, MIL-101Cr, with the same Cr−O cluster as MIL-100(Cr) and higher surface area, demonstrated a much lower $CO_2$ capacity of 2.19 mmol/g at 298 K and 1 bar. This is due to the larger pore size of MIL-101Cr, which is not good for small molecule adsorption and the lower density of unsaturated Cr sites (3.5 mmol/g) in MIL-101Cr vs 4.2 mmol/g in MIL-100(Cr) (Figure S4).

**3.2. Comparison of Isotherms on MIL-100(Cr) Powder and Pellets.** Adsorption isotherms of $CH_4$, $CO_2$, and $N_2$ at 298 K and 1 bar on MIL-100(Cr) samples, including powder and pellets activated at 423 and 523 K, are collected to understand the effects of the densification of MOF crystals on the adsorption capacity. As shown in Figure 5, MIL-100(Cr) pellets generally demonstrate less capacity than powder samples, in which the samples activated at 523 K present more loss than those activated at 423 K, indicating that the open Cr sites may tend to be blocked during the densification (the fitting data of Figure 5 are listed in Table S3 of the Supporting Information). In particular, powder MIL-100(Cr)-150 and pelletized MIL-100(Cr)150 did not show much

**Table 9. Transient Breakthrough Data of a $CO_2/N_2$ (20/80) Mixture in a Fixed-Bed Containing MIL-100(Cr)150 (a) and MIL-100(Cr)250 Pellets (b) at 298 K and 1 bar (5 mL/min)**

| MIL-100(Cr)150 | | | MIL-100(Cr)250 | | |
|---|---|---|---|---|---|
| time (min) | volume fraction % of $N_2$ | volume fraction % of $CO_2$ | time (min) | volume fraction % of $N_2$ | volume fraction % of $CO_2$ |
| 1 | 0 | 0 | 1 | 0 | 0 |
| 3 | 0 | 0 | 3 | 0 | 0 |
| 5 | 0 | 0 | 5 | 0 | 0 |
| 7 | 0 | 0 | 7 | 0 | 0 |
| 8 | 85 | 0 | 9 | 0 | 0 |
| 9 | 90 | 0 | 11 | 78 | 0 |
| 11 | 93 | 0 | 12 | 92 | 0 |
| 13 | 95 | 0 | 13 | 94 | 0 |
| 15 | 95 | 0 | 15 | 95 | 0 |
| 17 | 95 | 0 | 20 | 95 | 0 |
| 20 | 95 | 0 | 40 | 95 | 0 |
| 23 | 95 | 0 | 80 | 95 | 0 |
| 26 | 95 | 0 | 100 | 95 | 0 |
| 29 | 95 | 0 | 102 | 95 | 0 |
| 32 | 95 | 0 | 106 | 95 | 0 |
| 34 | 93 | 7 | 110 | 95 | 0 |
| 35 | 89 | 11 | 114 | 95 | 0 |
| 36 | 86 | 14 | 116 | 95 | 0 |
| 38 | 84 | 16 | 118 | 90 | 10 |
| 40 | 83 | 17 | 120 | 86 | 14 |
| 42 | 83 | 17 | 122 | 84 | 16 |
| 45 | 82 | 18 | 124 | 83 | 17 |
| 48 | 81 | 19 | 126 | 82 | 18 |
| 51 | 81 | 19 | 130 | 81 | 19 |
| 54 | 80 | 20 | 134 | 80 | 20 |
| 57 | 80 | 20 | 138 | 80 | 20 |
| 60 | 80 | 20 | 140 | 80 | 20 |

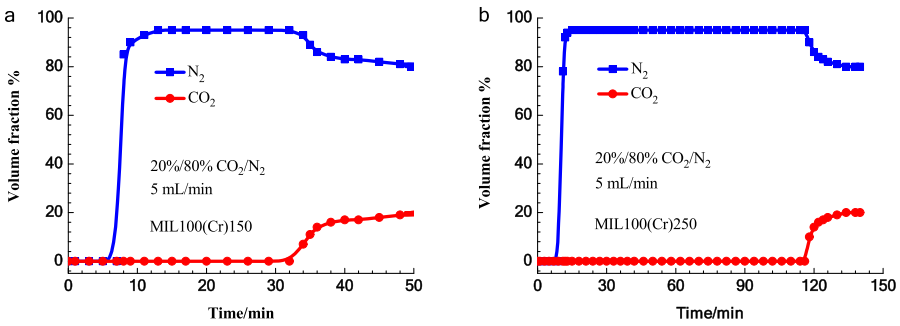


**Figure 6.** Transient breakthrough of a $CO_2/N_2$ (20/80) mixture in a fixed-bed containing MIL-100(Cr)150 pellets (a) and MIL-100(Cr)250 pellets (b) at 298 K and 1 bar.


DOI: 10.1021/acs.jced.9b00770
J. Chem. Eng. Data 2019, 64, 5814−5823

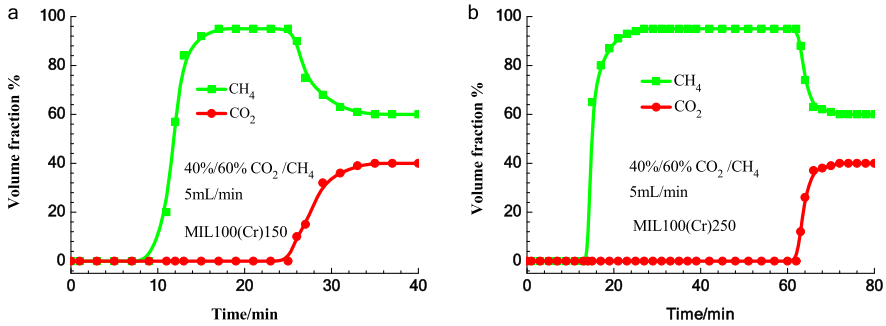


**Figure 7.** Transient breakthrough of a $CO_2/CH_4$ (40/60) mixture in a fixed-bed containing MIL-100(Cr)150 (a) and MIL-100(Cr)250 pellets (b) at 298 K and 1 bar.

**Table 10. Transient Breakthrough Data of a $CO_2/CH_4$ (40/60) Mixture in a Fixed-Bed Containing MIL-100(Cr)150 (a) and MIL-100(Cr)250 Pellets (b) at 298 K and 1 bar (5 mL/min)**

| MIL-100(Cr)150 | | | MIL-100(Cr)250 | | |
|---|---|---|---|---|---|
| time (min) | volume fraction % of $CH_4$ | volume fraction % of $CO_2$ | time (min) | volume fraction % of $CH_4$ | volume fraction % of $CO_2$ |
| 1 | 0 | 0 | 1 | 0 | 0 |
| 3 | 0 | 0 | 3 | 0 | 0 |
| 5 | 0 | 0 | 5 | 0 | 0 |
| 7 | 0 | 0 | 7 | 0 | 0 |
| 9 | 0 | 0 | 9 | 0 | 0 |
| 11 | 20 | 0 | 11 | 0 | 0 |
| 12 | 57 | 0 | 13 | 0 | 0 |
| 13 | 84 | 0 | 15 | 65 | 0 |
| 15 | 92 | 0 | 17 | 80 | 0 |
| 17 | 95 | 0 | 19 | 87 | 0 |
| 19 | 95 | 0 | 21 | 91 | 0 |
| 21 | 95 | 0 | 23 | 93 | 0 |
| 23 | 95 | 0 | 25 | 94 | 0 |
| 25 | 95 | 0 | 27 | 95 | 0 |
| 26 | 90 | 10 | 30 | 95 | 0 |
| 27 | 75 | 15 | 40 | 95 | 0 |
| 29 | 68 | 32 | 60 | 95 | 0 |
| 31 | 63 | 36 | 62 | 95 | 0 |
| 33 | 61 | 39 | 63 | 88 | 12 |
| 35 | 60 | 40 | 64 | 74 | 26 |
| 37 | 60 | 40 | 66 | 63 | 37 |
| 40 | 60 | 40 | 68 | 62 | 38 |
| | | | 70 | 61 | 39 |
| | | | 73 | 60 | 40 |
| | | | 77 | 60 | 40 |
| | | | 80 | 60 | 40 |

**Table 11. Breakthrough Time and Retention Time of $CO_2$ on MIL-100(Cr) Pellets**

| samples | gas mixture | breakthrough time (min) | retention time (min) | selectivity |
|---|---|---|---|---|
| MIL-100(Cr) 150 | $CO_2/N_2$ | 33 | 27 | 5.2 |
| | $CO_2/CH_4$ | 25 | 14 | 3.1 |
| MIL-100(Cr) 250 | $CO_2/N_2$ | 116 | 108 | 13.3 |
| | $CO_2/CH_4$ | 62 | 48 | 4.6 |

difference on $CO_2$ adsorption behavior, while a big drop on MIL-100(Cr)250 was observed, suggesting that 423 K could not open Cr sites, while 523 K does. The negative impact of densification on the adsorption capacity follows the order of $CO_2 > N_2 > CH_4$ for MIL-100(Cr)250 and $CH_4 > N_2 > CO_2$ for MIL-100(Cr)150, which also suggests that the effects of open Cr sites on the adsorption follow the order of $CO_2 > N_2 > CH_4$ on MIL-100(Cr). The adsorption data measured on the powder sample are listed in Table 6, while the data on pellets are presented in Table 7. The maximum value of each isotherm is listed in Table 8.

**3.3. Breakthrough Results of $CO_2/N_2$ Mixture on MIL-100(Cr) Pellets.** As mentioned before, the Cr−O ($CO_2$) distance in MIL-100(Cr) is estimated to be 2.24 Å, which is close to the Cr−N ($N_2$) distance (2.25 Å). However, the binding energy between Cr and $CO_2$ (63 kJ/mol) is higher than that between Cr and $N_2$ (48.7 kJ/mol), so we experimentally investigated the breakthrough behavior of $CO_2/N_2$ mixture on MIL-100(Cr)250 and MIL-100(Cr)150 samples, as shown in Figure 6a,b and Table 9 (adsorption capacity is summarized in Table S1). We observed that $N_2$ was eluted first, followed by $CO_2$ for both samples, clearly showing that MIL-100(Cr) strongly adsorbs $CO_2$ during the breakthrough. The steep nature of these curves is indicative of an efficient use of the adsorbent in dynamic processes. In the breakthrough study, two important parameters are the breakthrough time ($t_b$) and the corresponding uptake ($q_b$). In this work, $t_b$ is determined as the time corresponding to $C_A/C_o = 5\%$. The retention time of $CO_2$ on MIL-100(Cr)150 was 27 min, and this increased to 108 min on MIL-100(Cr)250, a 4-fold increase. In addition, the breakthrough selectivity of $CO_2/N_2$ (20/80) on MIL-100(Cr)150 and MIL-100(Cr)250 was 2.4 and 4.3, respectively (Table 11), indicating that MIL-100(Cr)250 was more efficient for the separation of the $CO_2/N_2$ (20/80) mixture. It is noteworthy that the equilibrium time of $CO_2$ and $N_2$ in this breakthrough test was very short, which is the advantage of using pellets as the adsorbents.

**3.4. Breakthrough Results of $CO_2/CH_4$ Mixture on MIL-100(Cr) Pellets.** The transient breakthrough test of the $CO_2/CH_4$ (40/60) mixture is shown in Figure 7 and Table 10 (adsorption capacity summary is shown in Table S1). The carbon dioxide adsorption retention time (48 min) of MIL-100(Cr)250 is about 3.4 times that of MIL-100(Cr)150. And the breakthrough selectivity of $CO_2/CH_4$ (40/60) on MIL-100(Cr)150 and MIL-100(Cr)250 is 4.2 and 10.7, respectively (Table 11). The breakthrough results were confirmed as MIL-100(Cr)250 was more efficient toward the separation of the $CO_2/CH_4$ (40/60) mixture. Remarkably, the equilibrium time of $CO_2$ and $CH_4$ in this breakthrough test was short, thus we can also infer that that is the advantage of using pellets as sorbents.


DOI: 10.1021/acs.jced.9b00770
J. Chem. Eng. Data 2019, 64, 5814−5823

## 4. CONCLUSIONS

The adsorption enthalpy of $CO_2$ on MIL-100(Cr) was estimated at around 63 kJ/mol, indicating its strong affinity to $CO_2$ molecules for separation applications. However, the previously reported $CO_2$ adsorption capacity at 298 K and 1 bar was not good enough (<4.0 mmol/g). Thus, in this study, we performed experiments to study the effects of activation temperature on MIL-100(Cr) adsorption performance and discovered that both a higher temperature (523−573 K) and high vacuum ($<10^{-10}$ bar) for 12 h activation time are required to open the Cr sites and achieve a capacity of 5.8−6.08 mmol/g at 298 K and 1 bar, which is the highest among the reported values. Isotherms were also collected on both MIL-100(Cr) powder and the pelletized form. The negative impact of densification on the adsorption capacity follows the order of $CO_2 > N_2 > CH_4$ for MIL-100(Cr)250 and $CH_4 > N_2 > CO_2$ for MIL-100(Cr)150, which also suggests that the effects of open Cr sites on the adsorption capacity follows the order of $CO_2 > N_2 > CH_4$ on MIL-100(Cr). Moreover, the mixed-gas breakthrough curves on MIL-100(Cr) pellets were measured to evaluate the real performance of this MOF for $CO_2/N_2$ and $CO_2/CH_4$ separation. The promising results demonstrate the great potential of properly activated MIL-100(Cr) for $CO_2$ separation applications.

## ■ ASSOCIATED CONTENT

### Supporting Information

The Supporting Information is available free of charge on the ACS Publications website at DOI: 10.1021/acs.jced.9b00770.

XRD patterns of examined samples; $N_2$ isotherms at 77 K; $CO_2$, $CH_4$, and $N_2$ adsorption isotherms of MIL-100(Cr) at 298 K (PDF)

## ■ AUTHOR INFORMATION


### Corresponding Author

*E-mail: bmu@asu.edu.

### ORCID

Yong Wang: 0000-0002-8002-4840

Bin Mu: 0000-0002-9117-1299


### Notes

The authors declare no competing financial interest.

## ■ ACKNOWLEDGMENTS

B.M. acknowledges financial support from the National Science Foundation (Grant Nos. CBET-1748641 and CMMI-1825594). J.Y. is grateful to the funding from the National Natural Science Foundation of China (Nos. 21676175 and 51672186).

## ■ REFERENCES


(1) Buhre, B. J. P.; Elliott, L. K.; Sheng, C. D.; Gupta, R. P.; Wall, T. F. Oxy-Fuel Combustion Technology for Coal-Fired Power Generation. *Prog. Energy Combust. Sci.* **2005**, *31*, 283−307.

(2) Wei, W.; Jinlong, G. Methanation of Carbon Dioxide: An Overview. *Front. Chem. Sci. Eng.* **2011**, *5*, 2−10.

(3) Rubin, E. S.; Mantripragada, H.; Marks, A.; Versteeg, P.; Kitchin, J. The Outlook for Improved Carbon Capture Technology. *Prog. Energy Combust. Sci.* **2012**, *38*, 630−671.

(4) Judd, S. J.; Al Momani, F. A. O.; Znad, H.; Al Ketife, A. M. D. The Cost Benefit of Algal Technology for Combined $CO_2$ Mitigation and Nutrient Abatement. *Renewable Sustainable Energy Rev.* **2017**, *71*, 379−387.

(5) Bui, M.; Adjiman, C. S.; Bardow, A.; Anthony, E. J.; Boston, A.; Brown, S.; Fennell, P. S.; Fuss, S.; Galindo, A.; Hackett, L. A.; et al. Carbon Capture and Storage (CCS): The Way Forward. *Energy Environ. Sci.* **2018**, *11*, 1062−1176.

(6) Arya, A.; Divekar, S.; Rawat, R.; Gupta, P.; Garg, M. O.; Dasgupta, S.; Nanoti, A.; Singh, R.; Xiao, P.; Webley, P. A. Upgrading Biogas at Low Pressure by Vacuum Swing Adsorption. *Ind. Eng. Chem. Res.* **2015**, *54*, 404−413.

(7) Shen, Y.; Ma, D.; Ge, X. $CO_2$-Looping in Biomass Pyrolysis or Gasification. *Sustainable Energy Fuels* **2017**, *1*, 1700−1729.

(8) Ji, G.; Yao, J. G.; Clough, P. T.; Da Costa, J. C. D.; Anthony, E. J.; Fennell, P. S.; Wang, W.; Zhao, M. Enhanced Hydrogen Production from Thermochemical Processes. *Energy Environ. Sci.* **2018**, *11*, 2647−2672.

(9) Gil, M. V.; Álvarez-Gutiérrez, N.; Martínez, M.; Rubiera, F.; Pevida, C.; Morán, A. Carbon Adsorbents for $CO_2$ Capture from Bio-Hydrogen and Biogas Streams: Breakthrough Adsorption Study. *Chem. Eng. J.* **2015**, *269*, 148−158.

(10) Canevesi, R. L. S.; Andreassen, K. A.; Da Silva, E. A.; Borba, C. E.; Grande, C. A. Pressure Swing Adsorption for Biogas Upgrading with Carbon Molecular Sieve. *Ind. Eng. Chem. Res.* **2018**, *57*, 8057−8067.

(11) Cui, Z.; Aroonwilas, A.; Veawab, A. Simultaneous Capture of Mercury and $CO_2$ in Amine-Based $CO_2$ Absorption Process. *Ind. Eng. Chem. Res.* **2010**, *49*, 12576−12586.

(12) Bos, M. J.; Kroeze, V.; Sutanto, S.; Brilman, D. W. F. Evaluating Regeneration Options of Solid Amine Sorbent for $CO_2$ Removal. *Ind. Eng. Chem. Res.* **2018**, *57*, 11141−11153.

(13) Karpe, P.; Aichele, C. P. Amine Modeling for $CO_2$ Capture: Internals Selection. *Environ. Sci. Technol.* **2013**, *47*, 3926−3932.

(14) Ling, H.; Gao, H.; Liang, Z. Comprehensive Solubility of $N_2O$ and Mass Transfer Studies on an Effective Reactive N, N-Dimethylethanolamine (Dmea) Solvent for Post-Combustion $CO_2$ Capture. *Chem. Eng. J.* **2019**, *355*, 369−379.

(15) Chen, X.; Huang, G.; An, C.; Yao, Y.; Zhao, S. Emerging N-Nitrosamines and N-Nitramines from Amine-Based Post-Combustion $CO_2$ Capture-a Review. *Chem. Eng. J.* **2018**, *335*, 921−935.

(16) Yang, J.; Li, J.; Wang, W.; Li, L.; Li, J. Adsorption of $CO_2$, $CH_4$, and $N_2$ on 8-, 10-, and 12-Membered Ring Hydrophobic Microporous High-Silica Zeolites: Ddr, Silicalite-1, and Beta. *Ind. Eng. Chem. Res.* **2013**, *52*, 17856−17864.

(17) Yang, J.; Shang, H.; Krishna, R.; Wang, Y.; Ouyang, K.; Li, J. Adjusting the Proportions of Extra-Framework $K^+$ and $Cs^+$ Cations to Construct a "Molecular Gate" on ZK-5 for $CO_2$ Removal. *Microporous Mesoporous Mater.* **2018**, *268*, 50−57.

(18) Yang, J.; Zhao, Q.; Xu, H.; Li, L.; Dong, J.; Li, J. Adsorption of $CO_2$, $CH_4$, and $N_2$ on Gas Diameter Grade Ion-Exchange Small Pore Zeolites. *J. Chem. Eng. Data* **2012**, *57*, 3701−3709.

(19) Zhang, P.; Zhong, Y.; Ding, J.; Wang, J.; Xu, M.; Deng, Q.; Zeng, Z.; Deng, S. A new choice of polymer precursor for solvent-free method: Preparation of N-enriched porous carbons for highly selective $CO_2$ capture. *Chem. Eng. J.* **2019**, *355*, 963−973.

(20) Wang, J.; Yang, J.; Krishna, R.; Yang, T.; Deng, S. A Versatile Synthesis of Metal-Organic Framework-Derived Porous Carbons for $CO_2$ Capture and Gas Separation. *J. Mater. Chem. A* **2016**, *4*, 19095−19106.

(21) Wang, J.; Zhang, P.; Liu, L.; Zhang, Y.; Yang, J.; Zeng, Z.; Deng, S. Controllable Synthesis of Bifunctional Porous Carbon for Efficient Gas-Mixture Separation and High-Performance Supercapacitor. *Chem. Eng. J.* **2018**, *348*, 57−66.

(22) Patiño, J.; Gutierrez, M. C.; Carriazo, D.; Ania, C. O.; Parra, J. B.; Ferrer, M. L.; Del Monte, F. Deep Eutectic Assisted Synthesis of Carbon Adsorbents Highly Suitable for Low-Pressure Separation of $CO_2$-$CH_4$ Gas Mixtures. *Energy Environ. Sci.* **2012**, *5*, 8699−8707.

(23) Zeng, Y.; Li, K.; Zhu, Q.; Wang, J.; Cao, Y.; Lu, S. Capture of $CO_2$ in Carbon Nanotube Bundles Supported with Room-Temperature Ionic Liquids: A Molecular Simulation Study. *Chem. Eng. Sci.* **2018**, *192*, 94−102.




DOI: 10.1021/acs.jced.9b00770
J. Chem. Eng. Data 2019, 64, 5814−5823

(24) Iqbal, N.; Wang, X.; Ahmed Babar, A.; Yu, J.; Ding, B. Highly flexible $NiCo_2O_4$/CNTs doped carbon nanofibers for $CO_2$ adsorption and supercapacitor electrodes. *J. Colloid Interface Sci.* **2016**, *476*, 87−93.
(25) Creamer, A. E.; Gao, B. Carbon-Based Adsorbents for Postcombustion $CO_2$ Capture: A Critical Review. *Environ. Sci. Technol.* **2016**, *50*, 7276−7289.
(26) Oschatz, M.; Antonietti, M. A Search for Selectivity to Enable $CO_2$ Capture with Porous Adsorbents. *Energy Environ. Sci.* **2018**, *11*, 57−70.
(27) Gargiulo, V.; Alfè, M.; Raganati, F.; Lisi, L.; Chirone, R.; Ammendola, P. BTC-based metal-organic frameworks: Correlation between relevant structural features and $CO_2$ adsorption performances. *Fuel* **2018**, *222*, 319−326.
(28) Ammendola, P.; Raganati, F.; Chirone, R. Effect of operating conditions on the $CO_2$ recovery from a fine activated carbon by means of TSA in a fluidized bed assisted by acoustic fields. *Fuel Process. Technol.* **2015**, *134*, 494−501.
(29) Gargiulo, V.; Alfè, M.; Ammendola, P.; Raganati, F.; Chirone, R. $CO_2$ sorption on surface-modified carbonaceous support: Probing the influence of the carbon black microporosity and surface polarity. *Appl. Surf. Sci.* **2016**, *360*, 329−337.
(30) Goel, C.; Kaur, H.; Bhunia, H.; Bajpai, P. K. Carbon dioxide adsorption on nitrogen enriched carbon adsorbents: Experimental, kinetics, isothermal and thermodynamic studies. *J. CO2 Util.* **2016**, *16*, 50−63.
(31) Raganati, F.; Alfe, M.; Gargiulo, V.; Chirone, R.; Ammendola, P. Isotherms and thermodynamics of $CO_2$ adsorption on a novel carbon-magnetite composite sorbent. *Chem. Eng. Res. Des.* **2018**, *134*, 540−552.
(32) Raganati, F.; Ammendola, P.; Chirone, R. On improving the $CO_2$ recovery efficiency of a conventional TSA process in a sound assisted fluidized bed by separating heating and purging. *Sep. Purif. Technol.* **2016**, *167*, 24−31.
(33) Loganathan, S.; Tikmani, M.; Edubilli, S.; Mishra, A.; Ghoshal, A. K. $CO_2$ adsorption kinetics on mesoporous silica under wide range of pressure and temperature. *Chem. Eng. J.* **2014**, *256*, 1−8.
(34) Álvarez-Gutiérrez, N.; Gil, M. V.; Rubiera, F.; Pevida, C. Kinetics of $CO_2$ adsorption on cherry stone-based carbons in $CO_2$/$CH_4$ separations. *Chem. Eng. J.* **2017**, *307*, 249−257.
(35) Serna-Guerrero, R.; Sayari, A. Modeling adsorption of $CO_2$ on amine-functionalized mesoporous silica. 2: Kinetics and breakthrough curves. *Chem. Eng. J.* **2010**, *161*, 182−190.
(36) Banerjee, R.; Phan, A.; Wang, B.; Knobler, C.; Furukawa, H.; O'Keeffe, M.; Yaghi, O. M. High-Throughput Synthesis of Zeolitic Imidazolate Frameworks and Application to $CO_2$ Capture. *Science* **2008**, *319*, 939−943.
(37) Zheng, S.; Bu, J. T.; Li, Y.; Wu, T.; Zuo, F.; Feng, P.; Bu, X. Pore Space Partition and Charge Separation in Cage-within-Cage Indium-Organic Frameworks with High $CO_2$ Uptake. *J. Am. Chem. Soc.* **2010**, *132*, 17062−17064.
(38) Zhang, J.; Wu, H.; Emge, T. J.; Li, J. A Flexible Mmof Exhibiting High Selectivity for $CO_2$ over $N_2$, $CH_4$ and Other Small Gases. *Chem. Commun.* **2010**, *46*, 9152−9154.
(39) Yang, J.; Wang, Y.; Li, L.; Zhang, Z.; Li, J. Protection of Open-Metal V(III) Sites and Their Associated $CO_2$/$CH_4$/$N_2$/$O_2$/$H_2O$ Adsorption Properties in Mesoporous V-Mofs. *J. Colloid Interface Sci.* **2015**, *456*, 197−205.
(40) Li, J.; Ma, Y.; McCarthy, M. C.; Sculley, J.; Yu, J.; Jeong, H.; Balbuena, P. B.; Zhou, H. Carbon Dioxide Capture-Related Gas Adsorption and Separation in Metal-Organic Frameworks. *Coord. Chem. Rev.* **2011**, *255*, 1791−1823.
(41) Li, J.; Sculley, J.; Zhou, H. Metal−Organic Frameworks for Separations. *Chem. Rev.* **2012**, *112*, 869−932.
(42) Belmabkhout, Y.; Guillerm, V.; Eddaoudi, M. Low Concentration $CO_2$ Capture Using Physical Adsorbents: Are Metal−Organic Frameworks Becoming the New Benchmark Materials? *Chem. Eng. J.* **2016**, *296*, 386−397.
(43) Bloch, E. D.; Murray, L. J.; Queen, W. L.; Chavan, S.; Maximoff, S. N.; Bigi, J. P.; Krishna, R.; Peterson, V. K.; Grandjean, F.; Long, G. J.; Place.; et al. Selective Binding of $O_2$ over $N_2$ in a Redox−Active Metal−Organic Framework with Open Iron(II) Coordination Sites. *J. Am. Chem. Soc.* **2011**, *133*, 14814−14822.
(44) Bloch, E. D.; Queen, W. L.; Krishna, R.; Zadrozny, J. M.; Brown, C. M.; Long, J. R. Hydrocarbon Separations in a Metal-Organic Framework with Open Iron(II) Coordination Sites. *Science* **2012**, *335*, 1606−1610.
(45) Murray, L. J.; Dinca, M.; Yano, J.; Chavan, S.; Bordiga, S.; Brown, C. M.; Long, J. R. Highly-Selective and Reversible $O_2$ Binding in $Cr_3$(1,3,5-Benzenetricarboxylate)$_2$. *J. Am. Chem. Soc.* **2010**, *132*, 7856−7857.
(46) Lou, W.; Yang, J.; Li, L.; Li, J. Adsorption and Separation of $CO_2$ on Fe(II)-MOF-74: Effect of the Open Metal Coordination Site. *J. Solid State Chem.* **2014**, *213*, 224−228.
(47) McDonald, T. M.; Mason, J. A.; Kong, X.; Bloch, E. D.; Gygi, D.; Dani, A.; Crocella, V.; Giordanino, F.; Odoh, S. O.; Drisdell, W. S.; Place.; et al. Cooperative Insertion of $CO_2$ in Diamine-Appended Metal-Organic Frameworks. *Nature* **2015**, *519*, 303−308.
(48) Bos, M. J.; Kroeze, V.; Sutanto, S.; Brilman, D. W. F. Evaluating Regeneration Options of Solid Amine Sorbent for $CO_2$ Removal. *Ind. Eng. Chem. Res.* **2018**, *57*, 11141−11153.
(49) Babaei, M.; Salehi, S.; Anbia, M.; Kazemipour, M. Improving $CO_2$ Adsorption Capacity and $CO_2$/$CH_4$ Selectivity with Amine Functionalization of MIL-100 and MIL-101. *J. Chem. Eng. Data* **2018**, *63*, 1657−1662.
(50) Zhang, F. F.; Shang, H.; Yang, J. F.; Ouyang, K.; Li, J. P. Ethylenediamine Modified Light Metal Aluminum-Metal-Organic Framework Material for $CO_2$/$CH_4$ Separation. *Chin. J. Inorg. Chem.* **2017**, *33*, 1611−1617.
(51) Cabello, C. P.; Berlier, G.; Magnacca, G.; Rumori, P.; Palomino, G. T. Enhanced $CO_2$ Adsorption Capacity of Amine-Functionalized MIL-100(Cr) Metal-Organic Frameworks. *CrystEngComm* **2015**, *17*, 430−437.
(52) Chen, B.; Ockwig, N. W.; Millward, A. R.; Contreras, D. S.; Yaghi, O. M. High $H_2$ Adsorption in a Microporous Metal−Organic Framework with Open Metal Sites. *Angew. Chem., Int. Ed.* **2005**, *44*, 4745−4749.
(53) Lin, L.; Kim, J.; Kong, X.; Scott, E.; McDonald, T. M.; Long, J. R.; Reimer, J. A.; Smit, B. Understanding $CO_2$ Dynamics in Metal−Organic Frameworks with Open Metal Sites. *Angew. Chem., Int. Ed.* **2013**, *52*, 4410−4413.
(54) Kim, H. K.; Yun, W. S.; Kim, M.; Kim, J. Y.; Bae, Y.; Lee, J.; Jeong, N. A Chemical Route to Activation of Open Metal Sites in the Copper-Based Metal−Organic Framework Materials HKUST-1 and Cu-MOF-2. *J. Am. Chem. Soc.* **2015**, *137*, 10009−10015.
(55) Férey, G.; Mellot-Draznieks, C.; Serre, C.; Millange, F.; Dutour, J.; Surble, S.; Margiolaki, I. A Chromium Terephthalate-Based Solid with Unusually Large Pore Volumes and Surface Area. *Science* **2005**, *309*, 2040−2042.
(56) Chui, S. S. -Y.; Lo, S. M. F.; Charmant, J. P.; Orpen, A. G.; Williams, I. D. A Chemically Functionalizable Nanoporous Material [$Cu_3(TMA)_2(H_2O)_3$]. *Science* **1999**, *283*, 1148−1150.
(57) Yu, D.; Yazaydin, A. O.; Lane, J. R.; Dietzel, P. D. C.; Snurr, R. Q. A combined experimental and quantum chemical study of $CO_2$ adsorption in the metal−organic framework CPO-27 with different metals. *Chem. Sci.* **2013**, *4*, 3544−3556.
(58) Queen, W. L.; Hudson, M. R.; Bloch, E. D.; Mason, J. A.; Gonzalez, M. I.; Lee, J. S.; Gygi, D.; Howe, J. D.; Lee, K.; Darwish, T. A.; Place.; et al. Comprehensive study of carbon dioxide adsorption in the metal−organic frameworks $M_2$(dobdc) (M = Mg, Mn, Fe, Co, Ni, Cu, Zn). *Chem. Sci.* **2014**, *5*, 4569−4581.
(59) Yoon, J. W.; Chang, H.; Lee, S.; Hwang, Y. K.; Hong, D.; Lee, S.; Lee, J. S.; Jang, S.; Yoon, T.; Kwac, K.; Place.; et al. Selective Nitrogen Capture by Porous Hybrid Materials Containing Accessible Transition Metal Ion Sites. *Nat. Mater.* **2017**, *16*, 526−531.


DOI: 10.1021/acs.jced.9b00770
J. Chem. Eng. Data 2019, 64, 5814−5823

(60) Yang, J.; Du, B.; Liu, J.; Krishna, R.; Zhang, F.; Zhou, W.; Wang, Y.; Li, J.; Chen, B. MIL-100Cr with open Cr sites for a record $N_2O$ capture. *Chem. Commun.* **2018**, *54*, 14061−14064.
(61) Nandasiri, M. I.; Jambovanea, S. R.; McGrailb, B. P.; Schaefc, H. T.; Nune, S. K. Adsorption, separation, and catalytic properties of densified metal-organic frameworks, Coordin. *Chem. Rev.* **2016**, *311*, 38−52.
(62) Zheng, J.; Cui, X.; Yang, Q.; Ren, Q.; Yang, Y.; Xing, H. Shaping of ultrahigh-loading MOF pellet with a strongly anti-tearing binder for gas separation and storage. *Chem. Eng. J.* **2018**, *354*, 1075−1082.
(63) Wickenheisser, M.; Herbst, A.; Tannert, R.; Milow, B.; Janiak, C. Hierarchical MOF-xerogel monolith composites from embedding MIL-100(Fe,Cr) and MIL-101(Cr) in resorcinol-formaldehyde xerogels for water adsorption applications. *Microporous Mesoporous Mater.* **2015**, *215*, 143−153.
(64) Blanita, G.; Coldea, I.; Misan, I.; Lupu, D. Hydrogen cryo-adsorption by hexagonal prism monoliths of MIL-101. *Int. J. Hydrogen Energy* **2014**, *39*, 17040−17046.
(65) Oh, H.; Lupu, D.; Blanita, G.; Hirscher, M. Experimental assessment of physical upper limit for hydrogen storage capacity at 20 K in densified MIL-101 monoliths. *RSC Adv.* **2014**, *4*, 2648−2651.
(66) Ardelean, O.; Blanita, G.; Borodi, G.; Lazar, M. D.; Misan, I.; Coldea, I.; Lupu, D. Volumetric hydrogen adsorption capacity of densified MIL-101 monoliths. *Int. J. Hydrogen Energy* **2013**, *38*, 7046−7055.
(67) Férey, G.; Serre, C.; Mellot-Draznieks, C.; Millange, F.; Surblé, S.; Dutour, J.; Margiolaki, I. A Hybrid Solid with Giant Pores Prepared by a Combination of Targeted Chemistry, Simulation, and Powder Diffraction. *Angew. Chem., Int. Ed.* **2004**, *43*, 6296−6301.
(68) Long, P.; Wu, H.; Zhao, Q.; Wang, Y.; Dong, J.; Li, J. Solvent Effect on the Synthesis of MIL-96 (Cr) and MIL-100 (Cr). *Microporous Mesoporous Mater.* **2011**, *142*, 489−493.
(69) Wu, L.; Xiao, J.; Wu, Y.; Xian, S.; Miao, G.; Wang, H.; Li, Z. A Combined Experimental/Computational Study on the Adsorption of Organosulfur Compounds over Metal−Organic Frameworks from Fuels. *Langmuir* **2014**, *30*, 1080−1088.
(70) Delley, B. From molecules to solids with the $DMol^3$ approach. *J. Chem. Phys.* **2000**, *113*, 7756−7764.
(71) Perdew, J. P.; Burke, K.; Ernzerhof, M. Generalized Gradient Approximation Made Simple. *Phys. Rev. Lett.* **1996**, *77*, 3865.
(72) Sun, Q.; Li, Z.; Searles, D. J.; Chen, Y.; Lu, G.; Du, A. Charge-Controlled Switchable $CO_2$ Capture on Boron Nitride Nanomaterials. *J. Am. Chem. Soc.* **2013**, *135*, 8246−8253.
(73) Liu, Y.; Liu, J.; Chang, M.; Zheng, C. Effect of Functionalized Linker on $CO_2$ Binding in Zeolitic Imidazolate Frameworks: Density Functional Theory Study. *J. Phys. Chem. C* **2012**, *116*, 16985−16991.
(74) Delley, B. Hardness conserving semilocal pseudopotentials. *Phys. Rev. B* **2002**, *66*, No. 155125.
(75) Pulay, P. Improved SCF convergence acceleration. *J. Comput. Chem.* **1982**, *3*, 556−560.
(76) Yang, J.; Krishna, R.; Li, J.; Li, J. Experiments and Simulations on Separating a $CO_2/CH_4$ Mixture Using K-KFI at Low and High Pressures. *Microporous Mesoporous Mater.* **2014**, *184*, 21−27.
(77) Llewellyn, P. L.; Bourrelly, S.; Serre, C.; Vimont, A.; Daturi, M.; Hamon, L.; De Weireld, G.; Chang, J.; Hong, D.; Hwang, Y. K.; Place.; et al. High Uptakes of $CO_2$ and $CH_4$ in Mesoporous Metal−Organic Frameworks MIL-100 and MIL-101. *Langmuir* **2008**, *24*, 7245−7250.
(78) Xian, S. K.; Peng, J. J.; Zhang, Z. J.; Xia, Q. B.; Wang, H. H.; Li, Z. Highly Enhanced and Weakened Adsorption Properties of Two Mofs by Water Vapor for Separation of $CO_2/CH_4$ and $CO_2/N_2$ Binary Mixtures. *Chem. Eng. J.* **2015**, *270*, 385−392.
(79) Li, L.; Yang, J.; Li, J.; Chen, Y.; Li, J. Separation of $CO_2/CH_4$ and $CH_4/N_2$ Mixtures by M/DOBDC: A Detailed Dynamic Comparison with MIL-100(Cr) and Activated Carbon. *Microporous Mesoporous Mater.* **2014**, *198*, 236−246.
(80) Hamon, L.; Heymans, N.; Llewellyn, P. L.; Guillerm, V.; Ghoufi, A.; Vaesen, S.; Maurin, G.; Serre, C.; De Weireld, G.; Pirngruber, G. D. Separation of $CO_2$-$CH_4$ Mixtures in the Mesoporous MIL-100(Cr) Mof: Experimental and Modelling Approaches. *Dalton Trans.* **2012**, *41*, 4052−4059.


DOI: 10.1021/acs.jced.9b00770
J. Chem. Eng. Data 2019, 64, 5814−5823